RSC Advances

PAPER

View Article Online
View Journal | View Issue

Open Access Article. Published on 27 August 2020. Downloaded on 1/14/2026 3:04:27 AM.
This article is licensed under a Creative Commons Attribution-NonCommercial 3.0 Unported Licence.

Check for updates

Cite this: *RSC Adv.*, 2020, **10**, 31780

Improved NO reduction by using metal–organic framework derived MnO_x–ZnO†

Ling Zhao,[*ab] Ziang Chen,[a] Peng Zhang[a] and Yu Zhang[a]

Received 9th May 2020
Accepted 18th August 2020

DOI: 10.1039/d0ra04161k

rsc.li/rsc-advances

Derivatives based on metal frameworks (MOFs) are attracting more and more attention in various research fields. MOF-based derivatives *x*% MnO_x–ZnO are easily synthesized by the thermal decomposition of Mn/MOF-5 precursors. Multiple technological characterizations have been conducted to ascertain the strengthening interaction between Mn species (Mn^{2+} or Mn^{3+}) and Zn^{2+} (*e.g.*, XRD, FTIR, TG, XPS, SEM, H_2-TPR and Py-FTIR). The 5% MnO_x–ZnO exhibits the highest NO conversion of 75.5% under C_3H_6-SCR. *In situ* FTIR and NO-TPD analysis showed that monodentate nitrates, bidentate nitrates, bridged bidentate nitrates, nitrosyl groups and $C_xH_yO_z$ species were formed on the surface, and further hydrocarbonates or carbonates were formed as intermediates, directly generating N_2, CO_2 and H_2O.

1. Introduction

Among the many problems related to air pollution, nitrogen oxides (NO_x), as pollutants, have received more and more attention from society owing to their increasing annual emissions and increasing harm. The massive emission of nitrogen oxides will not only cause acid rain and photochemical smog, but also cause a series of environmental problems such as the greenhouse effect and smog.[1,2] One of the main sources of NO_x is automobile fuel combustion. The selective catalytic reduction of NO_x by hydrocarbons has proved to be a cost-effective NO_x removal technology due to reducing NO_x and unburnt hydrocarbons simultaneously.[3,4] Many hydrocarbons have been used to increase the activity of HC-SCR (such as propylene,[5] ethanol,[6] methane,[7] ethylene,[8] propane,[9] *etc.*).

The term "metal–organic framework" (MOF) refers to an emerging class of porous crystalline materials fabricated by alternatively linking metal cations or metallic clusters to organic ligands in a 3D porous structure, and it has become a research hotspot due to their flexible structures, high void volume, large surface area, tailorable chemistry and for manifold applications (*e.g.*, catalysis, gas storage, adsorption and separation).[10–14] Nowadays, researchers have gradually shifted their focus from MOFs to MOFs derivatives.[15,17] Through high-temperature calcination, MOFs and their composite materials are gradually transformed into metal oxides from outside to inside. The resulting MOF-based derivatives not only inherit the porosity and good morphology from MOFs, but also have better thermal stability, therefore they will be good candidates for catalysts. Furthermore, the original MOFs doped or combined with another metal centres have received extensive attention, owing to their enhancing specific activity.[18–20] For instance, carbon-based catalyst for low temperature deoxygenation was prepared by Cu-based MOFs as precursors.[15] CeO_2 catalyst for toluene combustion was prepared by Ce-MOF.[16]

Mn had been demonstrated as a remarkable low-temperature SCR component due to variable valence, excellent redox capabilities and affluent Lewis acid sites, as well as less expensive and easily-obtained.[21,22] Manganese oxide contains various types of unstable oxygen and manganese oxidation states (Mn^{2+}, Mn^{3+} and Mn^{4+}), which is necessary and important for completing a catalytic cycle.[23] Hence, the Mn-based SCR catalyst has become a research hotspot. Kang *et al.* reviewed the important effects of MnO_x species and Mn valence state on the SCR process.[22] Deng *et al.* reported that the preferentially exposed (001) surface MnO_x/TiO_2 catalyst had a high NO conversion rate at 80–280 °C.[21]

In this work, a series of Mn/MOF-5 were successfully synthesized *via* a direct solvothermal method. Subsequently, ZnO and MnO_x–ZnO catalysts were synthesized by thermal decomposition of MOF-5 and Mn/MOF-5 precursors. Our main purpose is to evaluate the performance of the prepared MnO_x–ZnO catalyst in HC-SCR. C_3H_6 was acted as reducing agent as for it is the major hydrocarbons during the process of automobile exhaust emissions. Multi-technology characterizations were conducted to ascertain the properties of fabricated materials. Moreover, the adsorption and activation abilities of NO were carried out using fixed-bed quartz tube reactor and temperature-programmed desorption (TPD). On the basis of this, the C_3H_6-SCR process of fabricated materials was investigated and illuminated by dint of *in situ* Fourier transform infrared spectroscopy (*in situ* FTIR).

[a]*School of Ecology and Environment, Inner Mongolia University, China. E-mail: nmzhl@hotmail.com*

[b]*Center for Environmental and Human Toxicology, Department of Physiological Sciences, College of Veterinary Medicine, University of Florida, USA*

† Electronic supplementary information (ESI) available. See DOI: 10.1039/d0ra04161k

This journal is © The Royal Society of Chemistry 2020

Open Access Article. Published on 27 August 2020. Downloaded on 1/14/2026 3:04:27 AM.
This article is licensed under a Creative Commons Attribution-NonCommercial 3.0 Unported Licence.

2. Experimental

2.1. Catalyst preparation

MOF-5 was prepared from the classical solvothermal method. In a typical procedure, $Zn(NO_3)_2 \cdot 6H_2O$ (9.36 g) and H_2BDC (2.54 g) were dissolved in 190 mL DMF. The resulting mixture was equably stirred and then scattered in ultrasonic for 30 min at room temperature. Subsequently, the resulting mixture was transformed into Teflon-lined stainless steel sealed vessel (200 mL) and heated at 120 °C for 24 h. Then the product was cooled down to room temperature, and the precipitate was obtained by centrifugation and washed with DMF for three times and CH_2Cl_2 for twice. Afterwards, the product was dried at 80 °C for 12 h, followed by calcination at 600 °C for 4 h under air to obtain the catalyst of ZnO.

A wet impregnation technique was used to load Mn on a sample of the MOF-5. The mixture was kept at room temperature for over 24 h, then the $Mn(NO_3)_3$-loaded sample was calcinated at 600 °C for 4 h to obtain the catalysts of MnO_x–ZnO.

2.2. Catalysts characterization

Thermogravimetric (TG) curves were checked on SDT Q600 thermal analyzer under N_2 flow, over the range from room temperature to 800 °C. The X-ray diffraction (XRD) analysis for crystallographic structures were obtained on D8/ADVANCE diffractometer (Bruker) using Cu Kα radiation source (1.5406 Å) over the 2θ range of 10–80. Scanning electron microscopy (SEM) analysis was conducted on S-4800 field emission scanning electron microscope to study the surface morphology of the catalysts. FTIR and pyridine chemisorption spectra were obtained on a VERTEX 70 infrared spectrometer. The relative atomic compositions and elementary oxidation states were monitored by X-ray photoelectron spectroscopy (XPS) using ESCALABXI photoelectron spectrometer. Hydrogen temperature-programmed reduction (H_2-TPR) and NO temperature-programmed desorption (NO-TPD) data were conducted on a chemisorption analyzer (ChemBET TPR/TPD). Prior to the experiment, the sample (50 mg) was placed in a quartz U-type reactor and flushed with N_2 at 350 °C for 30 min to yield a clean surface followed by decreasing to target temperature. For TPR investigation, switching on 10 vol% H_2/Ar mixture for 30 min at normal temperature, and then carried out with a ramp of 10 °C min^{-1}, to 1000 °C.

2.3. Catalytic performance test

The catalytic activity was evaluated in a fixed-bed tubular reactor system (7 mm i.d.). The experiment was implemented with a steam contained 1000 ppm NO, 1000 ppm C_3H_6, 5 vol% O_2, and were balanced by He with a total flow rate was 150 mL min^{-1}. Prior to performing the C_3H_6-SCR, each sample (200 mg) was pretreated in He flow at 350 °C for 1 h. Subsequently, the reaction gas mixture was switched. Data was collected with a flue gas analyzer (Kane, British) when the airstream was stabled. The NO conversion percentage is calculated as follows:

$$\text{NO conversion} = ([NO]_{in} - [NO]_{out})/[NO]_{in} \times 100\%$$

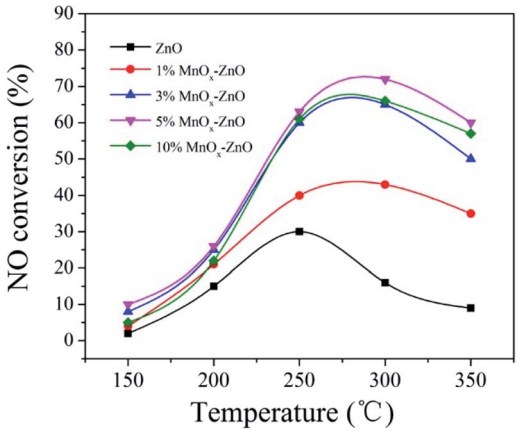

Fig. 1 NO conversion as a function of temperatures over ZnO and MnO_x–ZnO catalysts.

2.4. *In situ* FTIR measurements

In situ FTIR experiments were conducted at a FTIR spectrometer (Bruker VERTEX 70). Before the measurements, the sample wafers were mounted in the IR cell and activated at 400 °C for 30 min, then naturally cooled to 50 °C under high-purity He (50 mL min^{-1}) gas atmosphere. Collecting background spectrum of the solid and automatically deducted from the sample spectrum. The test gas conditions are: $[O_2] = 5$ vol%, $[NO] = [C_3H_6] = 1000$ ppm, which He is a balance gas.

3. Results and discussion

3.1. Catalytic test

The ZnO and MnO_x–ZnO samples derived from MOF-5 are evaluated in the SCR reactor under the testing conditions of NO and C_3H_6 (Fig. 1). For all research samples, it is noticed that the NO conversion changed with the increasing of reaction temperature (150–350 °C). The ZnO presented the maximum NO conversion of 31.5% when the temperature getting 250 °C, while a significant increase in activity of Mn doped samples was observed. Overall, 5% MnO_x–ZnO exhibited first-rank SCR performance with NO conversion reaching nearly 75.5% at 270 °C. Other documents also expounded some similar phenomena.[24,25] Xie *et al.* found that various MnO_x states played diverse roles in the selective catalytic reduction (SCR) with the temperature rising from 353 to 453 K.[24] Andreoli proposed that the Mn_3O_4 presence in the catalyst was the critical factor in obtaining activity.[25] On the other hand, the unsatisfactory performance of 10% MnO_x–ZnO (66.0%) may be due to the agglomeration of excess Mn on the catalyst surface. Furthermore, the 5% MnO_x–ZnO samples calcined with different times are evaluated in the SCR reactor at 275 °C and the curves of the catalytic activity are illustrated in Table 1. The results showed that all the 5% MnO_x–ZnO samples calcined at different times exhibited the similar NO conversion, which means that the calcination temperature has little influence on the NO conversion of the catalyst.

Open Access Article. Published on 27 August 2020. Downloaded on 1/14/2026 3:04:27 AM.
This article is licensed under a Creative Commons Attribution-NonCommercial 3.0 Unported Licence.

Table 1 Activity of various catalysts for C_3H_6-SCR

Catalyst	Calcination time	Reaction temperature (°C)	NO conversion (%)	Ref.
5% MnO_x–ZnO	600 °C for 2 h	275	72.1	This work
5% MnO_x–ZnO	600 °C for 4 h	275	75.5	This work
5% MnO_x–ZnO	600 °C for 6 h	275	75.1	This work
MA-MnO_x/TiO_2	600 °C in N_2	380	53.2	24
MA-MnO_x/TiO_2	600 °C in O_2	380	40.7	24
MA-MnO_x/TiO_2	600 °C in air	380	29.1	24
Mn_3O_4	400 °C for 1 h	275	70.3%	25

3.2. Physical and texture characterizations

The thermogravimetric curve of MOF-5 is illustrated in Fig. 2. It can be seen that the apparent loss of three weights. Between 50 and 100 °C, there is about 4% continuous weight loss resulting from moisture evaporation from the sample surface. Secondly, the evaporation and decomposition of residual organic components (DMF) happened between 150–320 °C.[26] The most significant weight loss occurred at temperatures above 420 °C, and the weight loss reached nearly 60% at an extremely fast rate, indicating that the skeleton of the MOF-5 has collapsed. Based on previous studies, for MOF-5, the break of the carboxyl bridge between the benzene ring and the Zn_4O cluster causes the organic ligand molecule to decompose into CO_2 and benzene,[11] and the material has been decomposed into the crystal ZnO. After 550 °C, the decomposition process is completed. Thermal weight analysis evidence proves that MOF-5 crystals can be completely converted to ZnO above 550 °C. Hence, 600 °C was determined as the calcination temperature.

According to the XRD diagram, we can confirm the transformation. Fig. 3(a) shows the representative diffraction peaks of MOF-5 material, of which 6.85°, 9.62°, 13.69°, 15.39° consistent with (200), (220), (400) and (420) planes.[11] The high crystallinity of MOF-5 material can be identified by the sharp peak at 6.85°.[11] In the meantime, from Fig. 3(b) we found that the initial framework structure collapsed in MOF-5 derived composites, the reflections locating at 31.7°(100), 34.4°(002), 36.3°(101), 47.4°(102), 56.6°(110), 62.8°(103), 67.9°(112) and 69.1°(201) were indexed to the characteristic peaks of wurtzite ZnO structure (JCPDS No. 36-1451).[26] Furthermore, no peaks of MnO_x phases were detected over 1% MnO_x–ZnO, 3% MnO_x–ZnO and 5% MnO_x–ZnO catalysts, which indicated that MnO_x species were highly dispersed over MOF-5 support or incorporated into MOF-5 lattice to form solid solution.[27] However, 10% MnO_x–ZnO sample displayed an additional XRD peak corresponded to the Mn_3O_4, indicating agglomeration of excess Mn compounds.

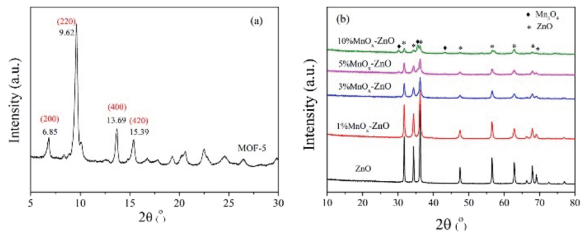

Fig. 3 XRD pattern of (a) MOF-5 and (b) ZnO and MnO_x–ZnO.

The FTIR spectra of the ZnO and MnO_x–ZnO catalysts derived from the MOF-5 were shown in Fig. 4. They show strong absorption peaks near 430 cm^{-1}, which is a sign of lattice vibrations of the Zn–O bond in ZnO.[28] In addition, the absorption peak of 1620 cm^{-1} is attributed to the OH bond bending vibration. The study of the absorption peak shows that the addition of Mn causes its ions to exist in the structure of MnO_x–ZnO cooperates with the carboxyl group, which will enhance the

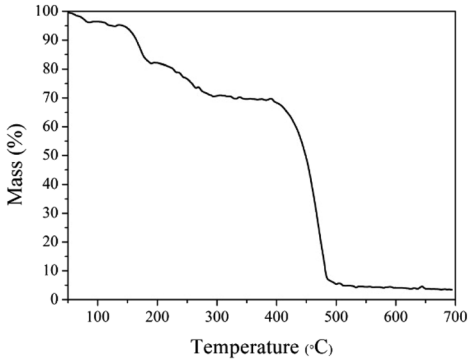

Fig. 2 The TG profile for the MOF-5 precursor.

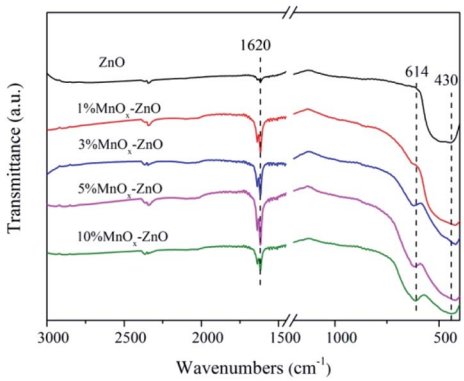

Fig. 4 FT-IR spectra of ZnO and MnO_x–ZnO catalysts.

Open Access Article. Published on 27 August 2020. Downloaded on 1/14/2026 3:04:27 AM.
This article is licensed under a Creative Commons Attribution-NonCommercial 3.0 Unported Licence.

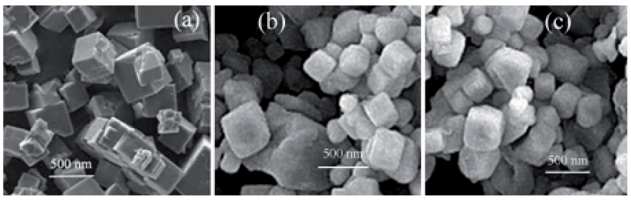

Fig. 5 SEM images of (a) MOF-5, (b) ZnO and (c) MnO_x–ZnO.

potential of the adsorption site. The interaction between these adsorption sites and the gas molecules to be adsorbed is further enhanced and the adsorption amount is increased. With the increase of the Mn content, the larger shift in the absorption peak at 614 cm^{-1} may be ascribed to the doping of Mn.

The scanning electron microscope photos of the catalysts are shown in Fig. 5. The MOF-5 sample clearly showed a cubic crystal shape with a smooth small surface, accompanied by a particle size range of 200 nm to 500 nm (Fig. 5(a)). Upon heating to 600 °C, the oxides (ZnO, MnO_x–ZnO) maintain a cubic structure, whereas the edges become smooth and the surface appears porous (Fig. 5(b) and (c)). Moreover, the particle size of the ZnO and MnO_x–ZnO catalysts decreased slightly compared to that of the MOF-5. As expected, when the MOF-5 and Mn/MOF-5 are heated, they gradually decompose over time, leading to smaller, porous and cubic particles.

The XPS spectra of Mn $2p_{3/2}$ are illustrated in Fig. 6(a). After a peak fitting deconvolution, the signal of Mn^{2+} (640.2 eV) and Mn^{4+} (645.5 eV) can be discovered. Previous literature reported that the redox process of Mn^{4+} species of vital importance in selective catalytic reaction with NH_3 at low-temperature (NH_3-SCR).[29] High Mn^{4+} concentration can promote the oxidation of NO to NO_2, thereby helping the NH_3-SCR processes through the "rapid SCR" approach.

Fig. 6(b) displayed the O 1s XPS spectra of ZnO and 5% MnO_x–ZnO samples, which were fitted into two different peaks representing surface lattice oxygen (O^{2-}) (530 eV, denoted as O_A) and surface chemisorbed oxygen or surface hydroxyl species (532.0 eV, denoted as O_B).[30,31] It is said that O^{2-} is the most active oxygen species and important for NO oxidation.[31] As shown in Fig. 6(b), for the 5% MnO_x–ZnO catalyst, its total superficial O surface concentration, especially O_A concentration is more than that of ZnO sample, which will promote the oxidation of NO to NO_2.

The H_2-TPR technology was employed in evaluating the reducibility of the catalysts. For all samples (Fig. 6), there are

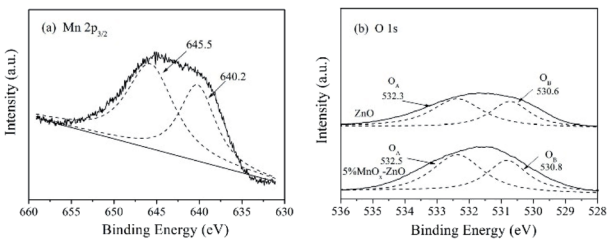

Fig. 6 XPS spectra for (a) Mn $2p_{3/2}$ of the 5% MnO_x–ZnO sample, (b) O 1s of the ZnO and 5% MnO_x–ZnO samples.

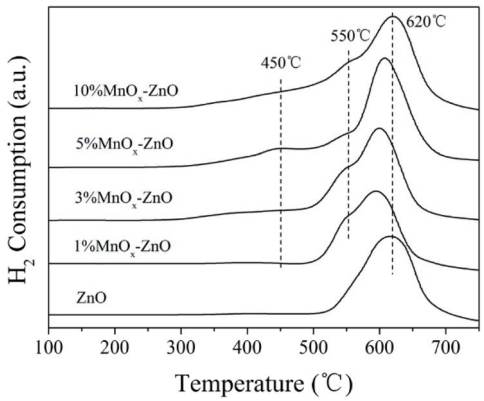

Fig. 7 H_2-TPR spectra of ZnO and MnO_x–ZnO catalysts.

one obvious peak centered at 620 °C. With the increase of manganese content, the redox performance of the MnO_x–ZnO catalysts have a clear transition to low temperatures, indicating that the redox performance of the catalysts is improved due to the interaction of ZnO and MnO_x. Moreover, two new H_2 desorption peaks could be observed over all MnO_x–ZnO catalysts. The first reduction peak at about 450 °C is due to the reduction of Mn_2O_3 to Mn_3O_4,[29] and the second reduction peak at 550 °C is attributed to the reduction of Mn_3O_4 to MnO.[29] The results reveal that the reduction performance of MnO_x–ZnO catalyst is stronger than that of ZnO. Following the enhanced redox performance could promote more NO being transferred and oxidated into NO_2 (Fig. 7).

3.3. NO-TPD measurements

To address the adsorption process, TPD-mass spectroscopy (MS) measurement were obtained. Fig. 8 shows the NO-TPD experiments for as-prepared catalysts. There are overlapped NO desorption peaks for all the samples, showing several NO adsorption species. The lower NO desorption temperatures between 176 and 208 °C could be attributed to physically

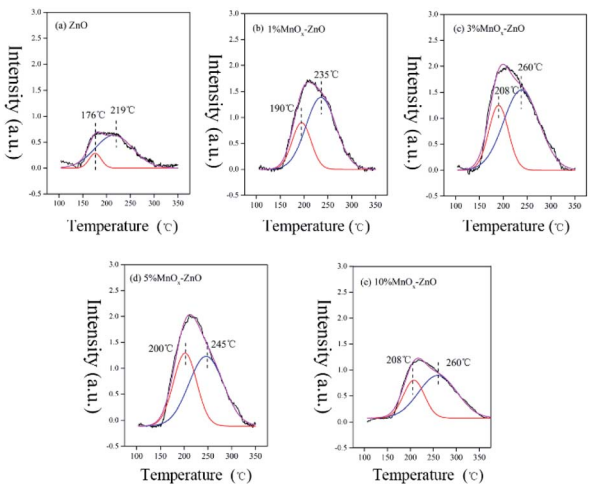

Fig. 8 NO-TPD profiles of ZnO and MnO_x–ZnO catalysts.

Open Access Article. Published on 27 August 2020. Downloaded on 1/14/2026 3:04:27 AM.
This article is licensed under a Creative Commons Attribution-NonCommercial 3.0 Unported Licence.

Table 2 Peak area of NO at ZnO and MnO_x–ZnO catalysts

Sample	Physical desorption peak area (a.u.)	Chemical desorption peak area (a.u.)	Total desorption peak area (a.u.)
ZnO	58.1	—	58.1
1% MnO_x–ZnO	45.0	109.2	154.2
3% MnO_x–ZnO	64.9	145.0	209.9
5% MnO_x–ZnO	110.1	156.3	266.3
10% MnO_x–ZnO	42.2	87.2	129.4

adsorbed NO, whereas the higher desorption peaks recorded between 219 and 260 °C could be assigned to strongly adsorbed NO and chemically adsorbed species (nitrate or nitrite).[32] Obviously, after Mn was added to the catalysts, the desorption peaks moved to a higher temperature, indicating that Mn can greatly enhance the bonding between NO and the catalyst surface. In addition, the desorption peak area of the manganese containing catalysts are significantly larger than that of the MOF-5 derived ZnO (Table 2), which indicates that the addition of Mn changes the chemical state of the catalyst surface, redistribution of adsorbed NO_x, thereby promoting the oxidation of NO. It is worth noting that after the Mn content reaches more than 10%, the promotion effect increases very slowly. This may be caused by excessive Mn agglomeration. On the whole, Mn doping could promote high dispersion of active species and further accelerate NO adsorptive and oxidative reaction. The results are well consistent with the data for catalytic test (Fig. 1).

3.4. Py-FTIR

Pyridine is one of the most widely used basic probe molecules to evaluate the nature and numbers of acidic centers. The FTIR spectra of pyridine chemisorbed on the ZnO and 5% MnO_x–ZnO catalysts evacuated at 250 °C are presented in Fig. 9. The catalysts displayed absorption peaks at wave numbers at 1464 and 1479 cm^{-1}, corresponding to the pyridine coordinated on Lewis acid sites.[30] The band at 1546 cm^{-1} was assigned to pyridinium cations formed after pyridine adsorption on Brønsted acid sites. Compared with ZnO catalyst, introduction of Mn led to the formation of Brønsted acid sites. Previous studies proposed that Brønsted acid sites favor NO reduction and are important SCR active sites as they can provide a reservoir of the reductant in the vicinity of the reduction site.[33] Therefore, the ZnO catalyst exhibited relatively weak NO adsorption strength and NO reduction ability, which agreed with the results of the catalytic test and NO-TPD results.

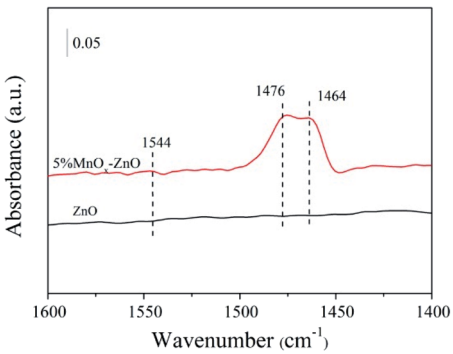

Fig. 9 *In situ* FTIR spectra of pyridine adsorbed on ZnO and 5% MnO_x–ZnO catalysts.

3.5. *In situ* FTIR studies

3.5.1. Adsorption of NO followed by C_3H_6/O_2 over time. *In situ* FTIR spectra were illustrated in Fig. 10, which were obtained by exposure to He of 1000 ppm NO and 5% O_2 at 250 °C

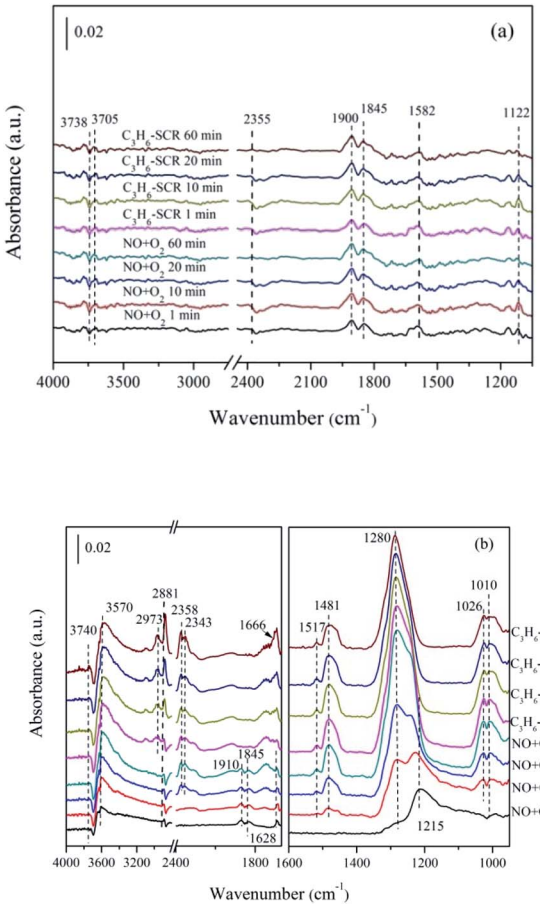

Fig. 10 *In situ* FTIR of (a) ZnO, (b) 5% MnO_x–ZnO exposed to the SCR reaction at 250 °C for various times under NO/O_2 adsorption and during C_3H_6 interaction with the NO/O_2 gas mixture.

Open Access Article. Published on 27 August 2020. Downloaded on 1/14/2026 3:04:27 AM.
This article is licensed under a Creative Commons Attribution-NonCommercial 3.0 Unported Licence.

followed by exposure to 1000 ppm C_3H_6 and 5% O_2. For ZnO catalyst derived from MOF-5, washing NO and O_2 at a temperature of 250 °C produces multiple bands (Fig. 10(a)). The characteristic peaks at 1122 cm^{-1} and 1582 cm^{-1} are assigned to the bidentate nitrates,[33,34] most probably they are formed when the NO molecule is bridged with two adjacent oxygen atoms.[33] Simultaneously, the bands related to nitrosyl (1845 cm^{-1} and 1900 cm^{-1}),[35,36] hydroxyl group (3705 cm^{-1} and 3738 cm^{-1})[35,36] and gas phase CO_2 (2355 cm^{-1})[37] were also observed. Switching the feed gas to C_3H_6/O_2, a slight decrease in the intensity of surface bidentate nitrates was appeared, while the other bands kept relatively stable.

As for 5% MnO_x–ZnO catalyst (Fig. 10(b)), monodentate nitrate (1010, 1026 and 1280 cm^{-1}), bidentate nitrate (1481 and 1517 cm^{-1}), bridge bidentate nitrate (1215 cm^{-1}), nitrosyl (at 1845 and 1910 cm^{-1}) and gas-phase NO (1628 cm^{-1}) species were formed after flushed by NO/O_2 for 10 min, indicating 5% MnO_x–ZnO exhibited better adsorption performance compared to MOF-5 derived ZnO sample. Introduction of C_3H_6/O_2 led to bridge bidentate nitrate (1215 cm^{-1}) and nitrosyl (1845 $cm^{-1}$and 1910 cm^{-1}) disappearance, and also resulted in part monodentate nitrate species decreasing (1010 cm^{-1}). In addition, there was no significant change in bidentate nitrates (at 1481 and 1517 cm^{-1}). The absorption peak of the bridged bidentate nitrate (1215 cm^{-1}) gradually increases to the maximum after 10 min, and then it was decreasing with the appearance and enhancement of the monodentate nitrate (1280 cm^{-1}). The results show that monodentate nitrate is converted from partially bridged bidentate nitrate.

Switching to C_3H_6/O_2 mixture, several new bands centered at 2973 and 2881 cm^{-1} were due to the asymmetric (ν_{as}) and symmetric (ν_{sym}) C–H stretching mode of CH_3 group, which had reported by Efstathiou' group to present $-CH_3$ group produced from the interplay between C_3H_6 and the catalyst surface.[38] Furthermore, the new band recorded at the 1660 cm^{-1} is correspond to the enolic species (RCH=CH–O–).[38] Besides, the bands with high intensity at 2343 cm^{-1} and 2358 cm^{-1} generated after C_3H_6 admission were attributed to gas phase CO_2. The band at 3570 cm^{-1} was due to the ν(OH) stretching of adsorbed H_2O.[30] The band at 3740 cm^{-1} was attributed to the vibrational modes of the surface hydroxyl species (OH).[39] It can be seen that the intensities of these bands increase significantly over time, which means that considerable amounts of CO_2 and H_2O are produced during the C_3H_6-SCR reaction. Actually, the increase of the $-CH_x$ was seemed controlled by the rate of propene dissociative chemisorption. According to the previous works,[35] the interplay between adsorbed NO and $-CH_x$ adsorbed species produced from C_3H_6 are key steps of C_3H_6-SCR. They reacted with each other and gave rise to CO_2, N_2 and H_2O.

3.5.2. Adsorption of C_3H_6/O_2 followed by NO/O_2 over time. The *in situ* FTIR spectra obtained after exposure to C_3H_6/O_2, followed by NO/O_2 over catalysts at 250 °C were investigated and the results were illustrated in Fig. 11. In this paper, 5% MnO_x–ZnO catalyst was taken as an example to analyze its flow spectrum. From Fig. 11 we can see the flushing of C_3H_6 + O_2 produced gas-phase C_3H_6 (at 1666 cm^{-1}) and –CH stretching vibration from unsaturated hydrocarbon fragments with bands centered at 3101 cm^{-1} and 2953 cm^{-1}. Subsequently, the NO/O_2 adsorption led to the gas-phase C_3H_6 and –CH stretching vibration declining. In addition, the bidentate nitrate (1481 cm^{-1}), nitrosyl (1843 and 1903 cm^{-1}) and gas-phase NO (1628 cm^{-1}) species were increased. Besides, a large amount for gas phase CO_2 was detected at 2358 and 2343 cm^{-1}.[30] The peaks at 3616 and 3727 cm^{-1} were attributed to the ν(OH) stretching of adsorbed H_2O.[30]

Previous study[38] has investigated that species produced by C_3H_6 adsorption on oxidic surfaces would further react with oxygen, which results in partial oxidation and formation of acrolein. Subsequently, acrolein is ulteriorly oxidized into $-CH_x$ from the acrylate ($C_xH_yO_z$) intermediate which is formed at the beginning. Our DRIFTS spectra results (Fig. 11) are in harmony with the above theory. The number of surface chemisorbed $-CH_x$ species is decreased by reacting with NO though hydrocarbonate species tend to decompose directly to CO_2, N_2 and H_2O.

3.5.3. Co-adsorption of NO + C_3H_6 over time. In order to clarity the surface reactions and intermediates, the *in situ* FTIR spectra of NO + C_3H_6 on catalysts in different time intervals at 250 °C are presented in Fig. 12. In the case of ZnO catalyst (Fig. 12(a)), NO and C_3H_6 flushing produced adsorbed bidentate nitrates (1582 and 1122 cm^{-1}),[33,34] nitrosyl (1845 cm^{-1} and

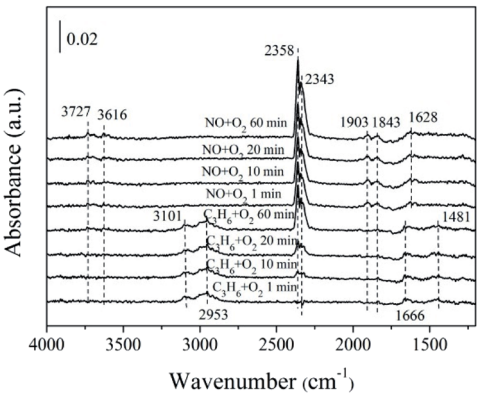

Fig. 11 *In situ* FTIR of 5% MnO_x–ZnO exposed to the SCR reaction at 250 °C for various times under C_3H_6/O_2 adsorption and during NO/O_2 interaction with the C_3H_6/O_2 gas mixture.

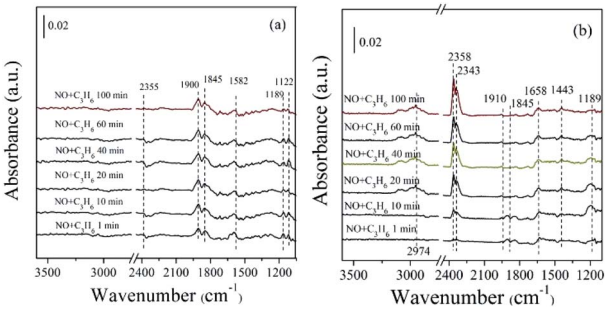

Fig. 12 *In situ* FTIR of (a) ZnO, (b) 5% MnO_x–ZnO exposed to the SCR reaction at 250 °C for various times under 1000 ppm NO + 1000 ppm C_3H_6.

Open Access Article. Published on 27 August 2020. Downloaded on 1/14/2026 3:04:27 AM.
This article is licensed under a Creative Commons Attribution-NonCommercial 3.0 Unported Licence.

1900 cm^{-1}),[35,36] and gas phase CO_2 (2355 cm^{-1}).[37] Along with the time increasing, the other bands kept relatively stable.

In the case of 5% MnO_x–ZnO catalyst (Fig. 12(b)), there are more plenty and kinds surface intermediates. The main species are bidentate nitrate (1443 cm^{-1}), bridge bidentate nitrate (1189 cm^{-1}), nitrosyl (1845 and 1900 cm^{-1}), enolic species (1658 cm^{-1}) and gas phase CO_2 (2358 and 2343 cm^{-1}). By comparing the adsorption amount of intermediate species, it can be concluded that the introduction of Mn promotes the adsorptive and active ability of catalyst for NO and C_3H_6.

3.6. Reaction pathway

The reaction mechanism can reveal the catalytic process and provide guidance for the improvement of catalyst performance.[39–42] Specifically, the proper introduction of manganese significantly boosts the catalytic performance. The reaction mechanism of the HC-SCR over MOF-5 derived MnO_x–ZnO catalysts conforms to the "reduction" mechanism scheme. It can be understood through analysis of XPS, H_2-TPR, NO-TPD and *in situ* FTIR. First, NO was adsorbed and subsequently oxidized with O_2 to NO_2 and stored in the form of bridged bidentate nitrates, nitrosyls, monodentate nitrates and bidentate nitrates at the Mn species or Zn^{2+} active sites. At the same time, a large number of $C_xH_yO_z$ (enolic species and acrylate) are formed and activated at these Mn species or Zn^{2+} active sites. Afterwards, the two kinds of intermediates above are active in the interaction with each other towards oxidation production (N_2, CO_2 and H_2O) *via* generation of hydrocarbonate or carbonate species. Combining with our present work, it is demonstrated that addition of Mn improves the formation of adsorbed NO_x substances and contributes to the improvement of C_3H_6-SCR activity due to increasing plenty of available active sites.

4. Conclusions

It is easy to synthesize MOF-based derivative x% MnO_x–ZnO (x = 1, 3, 5, 10) catalysts though thermal decomposition of Mn/MOF-5 precursor. The series of MnO_x–ZnO (x = 1, 3, 5, 10) catalysts are obtained upon calcination form the Mn/MOF-5 precursor. The physical and chemical properties of these catalysts were systematically studied with a series of comprehensive characterization. It is concluded that as-prepared MnO_x–ZnO can accelerate the interaction between Mn species (Mn^{2+} or Mn^{3+}) and Zn^{2+}. It was found that doping of manganese significantly improved the catalytic activity over catalysts. The 5% MnO_x–ZnO exhibits the highest NO conversion of 75.5% under C_3H_6-SCR. *In situ* FTIR and NO-TPD analysis showed that monodentate nitrates, bidentate nitrates, bridged bidentate nitrates, nitrosyl groups and $C_xH_yO_z$ species were formed on the surface, and further hydrocarbonate or carbonates were formed as intermediates.

Conflicts of interest

There are no conflicts to declare.

Acknowledgements

This study is supported by National Natural Science Foundation of China (No. 21866022, 21567018, 21347001), Inner Mongolia Natural Science Foundation (2017MS0214), Inner Mongolia Engineering Research Center of Coal Chemical Wastewater Treatment & Resourcelization.

References

1 Y. Mathieu, L. Tzanis, M. Soulard, J. Patarin, M. Vierling and M. Molière, *Fuel Process. Technol.*, 2013, **114**, 81–100.
2 J. N. Wang, Y. Lei, J. T. Yang and G. Yan, *Environ. Sci. Technol.*, 2012, **46**, 4263–4264.
3 N. A. S. Amin, E. F. Tan and Z. A. Manan, *J. Catal.*, 2004, **222**, 100–106.
4 X. Y. Liu, Z. Jiang, M. X. Chen, J. W. Shi, Z. X. Zhang and W. F. Shangguan, *Ind. Eng. Chem. Res.*, 2011, **50**, 7866–7873.
5 H. A. Habib, R. Basner, R. Brandenburg, U. Armbruster and A. Martin, *ACS Catal.*, 2014, 2479–2491.
6 H. Pan, Y. H. Guo, Y. F. Jian and C. He, *Energy Fuels*, 2015, **29**, 5282–5289.
7 G. Y. Xu, Y. B. Yu and H. He, *ACS Catal.*, 2018, **8**, 2699–2708.
8 Y. H. Hu and K. Griffiths, *Appl. Surf. Sci.*, 2008, **254**, 5048–5054.
9 K. Köhler and C. H. He, *J. Phys. Chem. C*, 2011, **115**, 1248–1254.
10 H. X. Jiang, Q. Y. Wang, H. Q. Wang, Y. F. Chen and M. H. Zhang, *ACS Appl. Mater. Interfaces*, 2016, **8**, 26817–26826.
11 L. Zhang and Y. H. Hu, *Mater. Sci. Eng., B*, 2011, **176**, 573–578.
12 W. Y. Huang, X. Zhou, Q. B. Xia, J. H. Peng, H. H. Wang and Z. Li, *Ind. Eng. Chem. Res.*, 2014, **53**, 11176–11184.
13 Z. J. Li, Y. L. Xiao, W. J. Xue, Q. Y. Yang and C. L. Zhong, *J. Phys. Chem. C*, 2015, **119**, 3674–3683.
14 Q. Naddaf, M. Mansour, H. Thakkar and F. Rezaei, *Ind. Eng. Chem. Res.*, 2018, **57**, 17470–17479.
15 L. Zhang, L. Huang, Y. H. Qin and B. Z. Chen, *Trans. Nonferrous Met. Soc. China*, 2018, **28**, 980–988.
16 X. Chen, X. Chen, E. Q. Yu, S. C. Cai, H. P. Jia, J. Chen and P. Liang, *Chem. Eng. J.*, 2018, **344**, 469–479.
17 K. Cendrowski, P. Skumial, P. Spera and E. Mijowska, *Mater. Des.*, 2016, **110**, 740–748.
18 A. Pariyar, H. Y. Asl and A. Choudhury, *Inorg. Chem.*, 2016, **55**, 9250–9257.
19 L. Wang, Y. Wu, R. Cao, L. Ren, M. Chen, X. Feng, J. Zhou and B. Wang, *ACS Appl. Mater. Interfaces*, 2016, **8**, 16736–16743.
20 H. Li, W. Shi, K. Zhao, H. Li, Y. Bing and P. Cheng, *Inorg. Chem.*, 2012, **51**, 9200–9207.
21 S. C. Deng, T. T. Meng, B. L. Xu, F. Gao, Y. H. Ding, L. Yu and Y. N. Fan, *ACS Catal.*, 2016, **6**, 5807–5815.
22 M. Kang, E. D. Park, J. M. Kim and J. E. Yie, *Appl. Catal.*, 2007, **327**, 261–269.
23 L. J. Yan, Y. Y. Liu, K. W. Zha, H. R. Li, L. Y. Shi and D. S. Zhang, *ACS Appl. Mater. Interfaces*, 2017, **9**, 2581–2593.

Open Access Article. Published on 27 August 2020. Downloaded on 1/14/2026 3:04:27 AM.
This article is licensed under a Creative Commons Attribution-NonCommercial 3.0 Unported Licence.

24 J. L. Xie, D. Fang, F. He, J. F. Chen, Z. B. Fu and X. L. Chen, *Catal. Commun.*, 2012, **28**, 77–81.
25 S. Andreoli, F. A. Deorsola, C. Galletti and R. Pirone, *Chem. Eng. J.*, 2015, **278**, 174–182.
26 A. V. Rajgure, N. L. Tarwal, J. Y. Patil, L. P. Chikhale, R. C. Pawar, C. S. Lee, I. S. Mulla and S. S. Suryavanshi, *Ceram. Int.*, 2014, **40**, 5837–5842.
27 X. H. Li, S. L. Zhang, Y. Jia, X. X. Liu and Q. Zhong, *J. Nat. Gas Chem.*, 2012, **21**, 17–24.
28 R. Sabouni, H. Kazemian and S. Rohani, *Chem. Eng. J.*, 2010, **165**, 966–973.
29 D. Fang, J. L. Xie, H. Hu, H. Yang, F. He and Z. B. Fu, *Chem. Eng. J.*, 2015, **271**, 23–30.
30 L. Zhao, X. Y. Li, X. Quan and G. H. Chen, *Environ. Sci. Technol.*, 2011, **45**, 5373–5379.
31 F. Liu, H. He and Y. Ding, *Appl. Catal., B*, 2009, **93**, 194–204.
32 H. Teng, L. Hsu and Y. Lai, *Environ. Sci. Technol.*, 2001, **35**, 2369–2374.
33 J. Liu, X. Y. Li, Q. D. Zhao, C. Hao and D. K. Zhang, *Environ. Sci. Technol.*, 2013, **47**, 4528–4535.
34 K. Ueda, J. Y. Ohyama and A. Satsuma, *ACS Omega*, 2017, **2**, 3135–3143.
35 W. Yang, R. D. Zhang, B. H. Chen, D. Duprez and S. Royer, *Environ. Sci. Technol.*, 2012, **46**, 11280–11288.
36 J. Liu, X. Y. Li, Q. D. Zhao, C. Hao, S. B. Wang and M. Tade, *ACS Catal.*, 2014, **4**, 2426–2436.
37 X. X. Cheng, Y. R. Cheng, Z. Q. Wang and C. Y. Ma, *Fuel*, 2018, **214**, 230–241.
38 C. M. Kalamaras, G. G. Olympiou, V. I. Pârvulescu, B. Cojocaru and A. M. Efstathiou, *Appl. Catal., B*, 2017, **206**, 308–318.
39 J. L. Long, Z. Z. Zhang, Z. X. Ding, R. S. Ruan, Z. H. Li and X. X. Wang, *J. Phys. Chem. C*, 2010, **114**, 15713–15727.
40 M. Haneda, N. Bion, M. Daturi, J. Saussey, J. C. Lavalley, D. Duprez and H. Hamada, *J. Catal.*, 2002, **206**, 114–124.
41 R. Burch, J. P. Breen and F. C. Meunier, *Appl. Catal., B*, 2002, **39**, 283–303.
42 H. Hu, K. W. Zha, H. R. Li, L. Y. Shi and D. S. Zhang, *Appl. Surf. Sci.*, 2016, **387**, 921–928.